

A Proposal to JLab PAC 42, a companion to the WACS Proposal

Wide Angle, Exclusive Photoproduction of π^0 Mesons

J. Dunne, D. Dutta (Co-spokesperson and contact person)
Mississippi State University, Mississippi State, MS

H. Gao (Co-spokesperson)
Duke University and Triangle University Nuclear Lab, Durham, NC

S. Širca (Co-spokesperson)
University of Ljubljana, Ljubljana, Slovenia

M. Amarian (Co-spokesperson) and M. Kunkel (Co-spokesperson)
Old Dominion University, Norfolk, VA

I. Strakovsky (Co-spokesperson)
George Washington University, Washington, DC

The Wide Angle Compton Scattering (RCS) collaboration
and
the Neutral Particle Spectrometer (NPS) collaboration

The study of the short range structure of the nucleon through generalized parton distributions and the handbag mechanism is a central part of the research program at Jefferson Lab. It is widely accepted that this new framework needs to be studied using wide angle exclusive processes such as Compton scattering and pion photoproduction at large angles. The $\gamma p \rightarrow \pi^0 p$ reaction is the next simplest real photon induced exclusive process after Compton Scattering and is thus an essential reaction to examine the validity of the “handbag” mechanism and soft-hard factorization. The ratio of neutral to charged pions can be used to test models based on the dominance of the “handbag” mechanism. However, before the measured cross section and ratios can be compared to theoretical calculations the large discrepancy between existing data sets must be resolved. The proposed measurement will enable a precise extraction of the cross section using a technique with completely different systematics compared to previous measurements. The cross section at large pion center-of-mass angles will also allow detailed investigation of the angular dependence of the onset of scaling in photopion production. The 11 GeV CEBAF beam enables investigation of this process across the J/Ψ threshold and help verify predictions involving the opening of the $uud\bar{u}d\bar{c}\bar{c}$ resonance states.

We propose to measure the differential cross section of the $\gamma p \rightarrow \pi^0 p$ process for photon energies between 6 GeV to 11 GeV at large pion center-of-mass angles of $55^\circ < \theta_{CM} < 105^\circ$. The proposed measurements will be carried out in Hall C using an electron beam impinging on a 6% copper radiator and a liquid hydrogen target. The recoil proton will be detected in the HMS spectrometer and photons from the $\pi^0 \rightarrow \gamma\gamma$ decay will be detected in the Neutral Pion Spectrometer (NPS) which is under construction. The scattered electrons will be deflected by using a sweeping magnet.

This is a companion to the proposed wide angle Compton scattering (WACS) experiment. We propose to extract the π^0 cross section from the same data set that is collected by the WACS experiment. In addition to all of the settings of the WACS experiment measurements at a beam energy of 6.6 GeV will be required for the proposed experiment.

CONTENTS

Introduction	3
Physics Motivation	5
The Handbag Mechanism and GPD-based Models	7
Constituent Counting Rule	11
Generalized counting rule	12
Is oscillatory scaling behavior unique to proton-proton elastic scattering?	14
Summary of motivations	15
The Proposed Measurement	15
The CEBAF Electron Beam	15
Target and Radiator	16
Deflection Magnet	16
The High Momentum Spectrometer	18
Expected Rates	18
The Photon Calorimeter	19
Expected Rates	20
Trigger and DAQ	20
Radiation Budget	21
Energy and Coordinate Resolution	21
Kinematic settings	22
Monte Carlo Simulation	23
Physics Background	25
Detector Resolution	26
Rates and Systematic Uncertainties	26
Beam Time Request	28
Projected Results	28
Summary	29
References	30

INTRODUCTION

Exclusive processes at large momentum transfers and wide angles ($p_T \geq 1\text{GeV}/c$) are essential for studies of the short range structure of nucleons. They provide a robust testing ground for QCD at intermediate energies which is one of the main goals of the physics program at JLab. Towards this goal, wide angle exclusive processes can be used to test recent developments, such as the framework based on the dominance of the “handbag mechanism” and models based on Generalized Parton Distribution (GPD) [1]. Given the relatively large cross sections for pion photoproduction, a confirmation of the dominance of the handbag mechanism would enable a study of the nucleon structure at large values of W and $-t$.

The handbag mechanism for wide-angle scattering reactions was first developed for Compton scattering [2, 3] and subsequently applied to photo- and electroproduction of mesons [4]. Several new calculations on wide-angle Compton scattering have recently become available [?] and they can reproduce the measured cross sections. After Compton scattering, pion photoproduction is the next simplest realphoton induced exclusive process. Although calculations of the pion photoproduction cross sections tend to disagree with experiments by orders of magnitude, H. Huang *et al.* [9] have calculated ratios of charged to neutral pions and ratios of positive to negatively charged pions, which can be used to test the validity of the handbag mechanism. But, the neutral pion data available at the highest energies have large discrepancies between different data sets, as seen in Fig. 1 which makes it impossible to extract ratios that can be compared to predictions. The current situation can only be remedied with a new measurements that employs a new technique with a new high resolution and radiation hard neutral pion detector [10] along with the high luminosity that will be available at JLab Hall-C. Since the neutral pion is one of the dominant backgrounds for the proposed WACS experiment, this proposal uses the exact same setup and is a companion to the WACS proposal [11]. Moreover, for neutral to charged pion ratios, we require the charged pion production data from the G_E^n and G_M^n experiments in Hall-A. These experiments will use the SBS and Big Hand detector and plan to utilize the charged pion production for calibration.

Wide-angle exclusive processes can also help understand the transitions from the non-perturbative to perturbative regime of QCD. The differential cross sections for many exclusive reactions [13] at high energy and large momentum transfer appear to obey the quark counting rule [14]. The quark counting rule was originally obtained based on dimensional analysis of typical renormalizable theories. The same rule was later obtained in a short-distance perturbative QCD approach by Brodsky and Lepage[15]. Despite many successes, a model-independent test of the approach, called the hadron helicity conservation rule, tends not to agree with data in the similar energy and momentum region. It has been suggested that contributions from nonzero parton orbital angular momentum could break the hadron helicity conservation rule [16], although these contributions are power suppressed [15]. In addition some of the cross-section data can also be explained in terms of non-perturbative calculations [17]. Recent developments, such as the generalized counting rule proposed by Ji *et al.* [18], the derivation of the quark-counting rule from the anti-de Sitter/Conformal Field Theory (AdS/CFT) correspondence [19], and the machinery to compute the hadronic light front wave functions developed by Brodsky *et al.* [20], have focused interest back on this subject.

The scaling behavior has been studied extensively in deuteron photo-disintegration experiments at SLAC and JLab [24] - [27]. Onset of the scaling behavior has been observed in deuteron photo-disintegration [26, 27] at a surprisingly low momentum transfer of $1.0 (\text{GeV}/c)^2$ to the nucleon. Scaling behavior has also been observed in pion photoproduction, most recently in neutral pion production as shown in Fig. 2. However, a polarization measurement on deuteron photo-

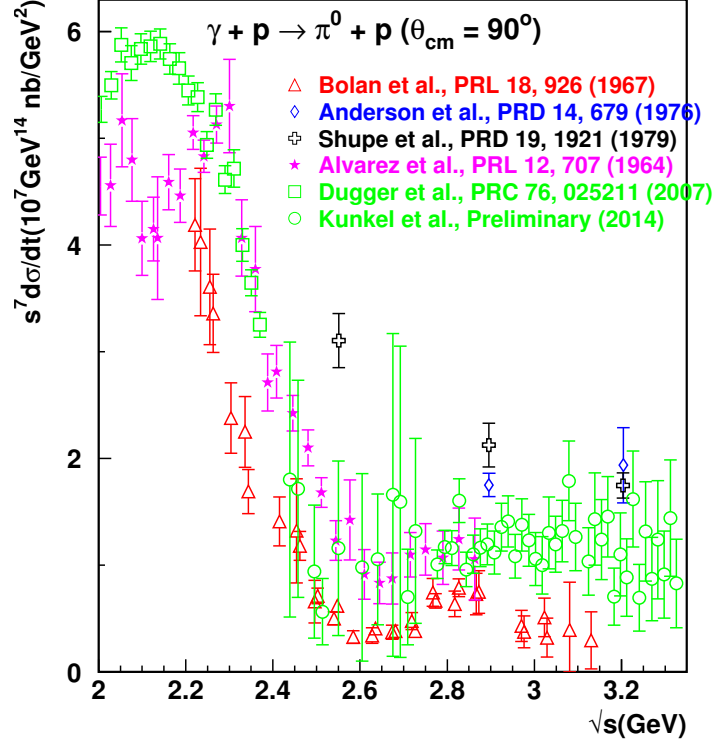


FIG. 1. The scaled differential cross section, $s^7 \frac{d\sigma}{dt}$ as a function of \sqrt{s} at a center-of-mass angle of 90° for $\gamma p \rightarrow \pi^0 p$ at the highest energies.

disintegration [28] and in neutral pion photo-production [29, 30], shows disagreement with hadron helicity conservation in the same kinematic region where the quark counting behavior is apparently observed. These paradoxes make it essential to understand the exact mechanism governing the early onset of scaling behavior. Towards this goal, it is important to look closely at claims of agreement between the differential cross section data and the quark counting prediction and also to examine it over large angular range. The scaled 90° center-of-mass pp elastic scattering data, $s^{10} \frac{d\sigma}{dt}$ show substantial oscillations about the power law behavior. Oscillations may not be restricted to the pp sector; they are also seen in πp fixed angle scattering [31]; the older [32, 33] as well as the more recent JLab data [34] on photo production of charged pions, at $\theta_{cms} = 90^\circ$ also show hints of oscillation about the s^{-7} scaling; see for example Fig. 3. Thus, it is essential to confirm and map out the oscillatory scaling behavior. The relatively large pion photoproduction cross section will allow us to perform a fine energy and angular scan.

A large fraction of the pion photoproduction data at the highest energies have been collected using the “bremsstrahlung end point” technique. At the upgraded JLab, because of the fixed electron beam energy the end point technique would be restricted to very narrow range of energies and is thus no longer very productive. A high resolution, radiation-hard neutral particle detection

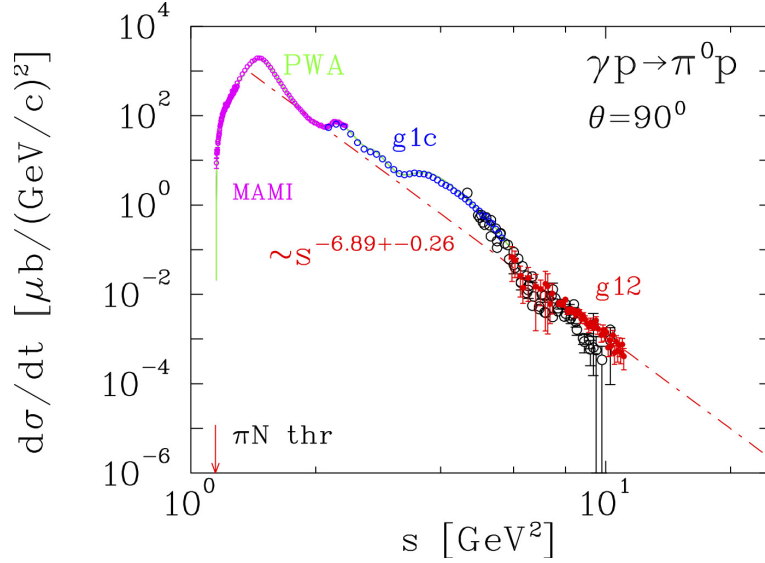


FIG. 2. The differential cross section for the $\gamma p \rightarrow \pi^0 p$ reaction at $\theta_{CM} = 90^\circ$, as a function of the center of mass energy. The data are from Ref. [21], [22] and [23]. The red points are preliminary results from a recent analysis of the CLAS g12 data. At the highest energies the results are consistent with the s^{-7} scaling expected from the quark counting rule.

facility will provide an alternative method to measure wide angle π^0 photoproduction. The Neutral Pion Spectrometer under construction in Hall-C exactly fits the bill and will enable us to test the reaction mechanism of π^0 photoproduction. We propose to measure the differential cross-section $\frac{d\sigma}{dt}$ for the $p(\gamma, \pi^0)p$ processes over a range of center-of-mass angles in a photon energy between 5.0 and 11 GeV. We propose to use the data collected by the WACS experiment [11] at $E_{beam} = 8.8$ and 11.0 GeV to extract the π^0 cross section which is the largest source of background for the WACS experiment. In addition we propose to use the setup of the WACS experiment for additional measurements with 6.6 GeV electron beam at $50^\circ \leq \theta_{CM} \leq 105^\circ$. Using the high luminosity and energy upgraded CEBAF, one can verify the dominance of the handbag mechanism in pion photoproduction and also investigate its scaling behavior in detail to help identify the exact nature and the underlying mechanism responsible for scaling. For example, is it caused by the quark orbital angular momentum effect seen in the generalized quark counting rule [18] or due to the opening of new charm resonance [35] states? The 11 GeV CEBAF will allow measurements across the charm threshold.

PHYSICS MOTIVATION

The main physics goals for measuring the π^0 cross section using the new NPS facility are to address the following questions:

1. Does the exclusive photopion production reaction proceed through the interaction of the photon with a single quark?
2. What is the energy scale for the transition from non-perturbative to perturbative mechanisms

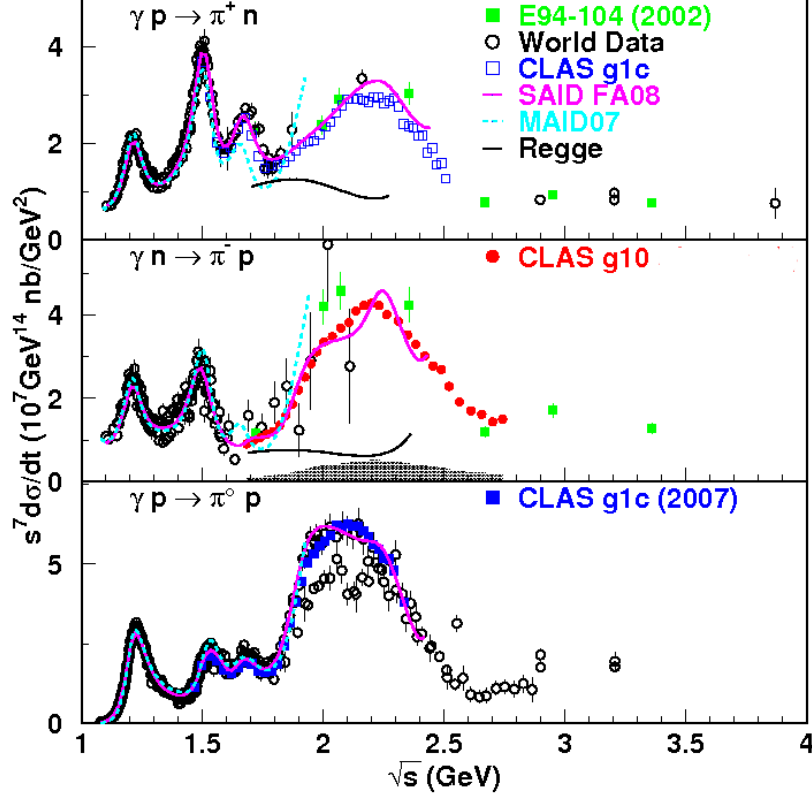


FIG. 3. The scaled differential cross section, $s^7 \frac{d\sigma}{dt}$ as a function of \sqrt{s} at a center-of-mass angle of 90° for $\gamma p \rightarrow \pi^+ n$ channel (top panel), the $\gamma n \rightarrow \pi^- p$ channel (middle panel) and $\gamma p \rightarrow \pi^0 p$ (bottom panel). The data from JLab E94-104 are shown as green solid squares [34] and the CLAS π^+ data [36] are shown as magenta open squares, the π^- results [37] are shown as red solid circles and the π^0 results [38] are shown as magenta solid squares. The SAID SP09 results [39] are shown as the blue solid curves in all three panels. The prediction from a Regge approach [40] is shown in the top and middle panels by black solid curves. The black open circles are the world data collected from Refs. [32, 33]

and/or soft to hard factorization mechanisms?

3. What can we learn about the non-perturbative structure of the proton using wide angle exclusive processes in general and pion photoproduction in particular?

We briefly discuss the current status of pion photoproduction models and the existing data and what is needed to be able to address the questions posed above.

The Handbag Mechanism and GPD-based Models

The introduction of the handbag mechanism has provided new possibilities for the interpretation of hard exclusive reactions. In this approach, the reaction is factorized into two parts, one quark from the incoming and one from the outgoing nucleon participate in the hard sub process, which is calculable using pQCD. While the soft part consists of all the other partons that are spectators and can be described in terms of GPDs [1]. This is illustrated in Fig. 4, where the hard exclusive meson (M) photo-production process factorizes into, $\gamma + q \rightarrow Mq$ and GPDs describing the soft hadronparton transitions. The handbag mechanism is applicable when the Mandelstam variables, s, t, u , are large as compared to a hadronic scale of order 1 GeV . The GPDs contain a wealth of

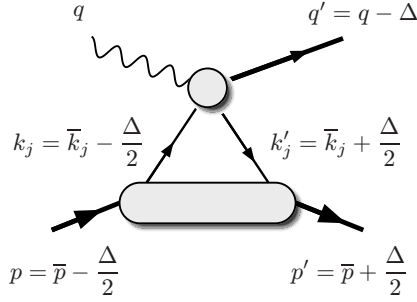


FIG. 4. The handbag diagram for photoproduction of mesons. The large blob represents a baryon GPD, while the small one stands for meson photoproduction off quarks.

information about the transverse distance and angular momentum of the quarks in the proton. They provide a unified description of nucleon structure, a common framework that can be applied to inclusive, semi-inclusive, and exclusive reactions. Presently, experimental access to such GPDs is amongst the highest priorities in intermediate energy nuclear/particle physics. However, access to the GPDs is intrinsically related to the soft-hard factorization. All order proofs of factorisation exists only for deeply virtual processes. Factorization is particularly simple in the wide-angle processes, where it has been shown to hold to next-to-leading order in Compton scattering and to leading order in photoproduction of mesons. However, it is still uncertain at which Q^2 value one will reach the factorization regime, where leading-order perturbative QCD is fully applicable.

Recently, a new GPD based calculation by Diehl and Kroll [8] for wide angle Compton scattering, has been shown to agree with experimental data (see Fig. 5). The photoproduction of neutral pions at large C.M. angles is the next simplest reaction that can be tested against these GPD models. However, calculations of the pion photoproduction cross sections fail to describe the experimental data by an order of magnitude [4]. It is considered that this failure maybe because of the one-gluon exchange mechanism for the generation of the meson and not the handbag mechanism itself. Although, the cross sections do not match experiments, recently H.W.Huang *et al.*, have also calculated other signatures of the handbag mechanism in wide-angle photoproduction of pseudoscalar mesons [9]. Their calculation is carried out in a symmetrical CMS frame where the incoming (p) and outgoing (p') baryons have the same light-cone plus components and the skewness ξ vanish. Within the handbag approach, they make use of the fact that that the subprocess Mandelstam variables \hat{s} and \hat{u} are the same as the ones for the full process (s and u). Additionally, there are ambiguities in relating the massless kinematics used in the handbag approach with the experimental ones, in particular at energies available at JLab, hence the proton mass cannot be

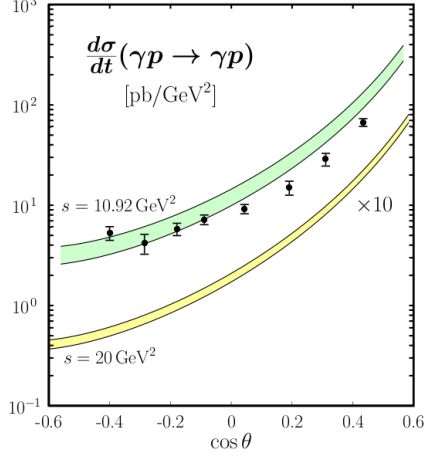


FIG. 5. The Compton cross section at $s = 10.92$ and 20 GeV^2 , evaluated in Ref. [8] compared to data from JLab.

ignored. The nucleon mass is taken into account properly using [41]:

$$s = s_{\text{exp}} - m^2, \quad t = t_{\text{exp}}, \quad u = u_{\text{exp}} - m^2. \quad (1)$$

where s_{exp} , u_{exp} , t_{exp} are the Mandelstam variables of the experiment.

The meson photoproduction is represented as a hard parton-level subprocess $\gamma q_a \rightarrow P q_b$ and a soft emission and reabsorption of quarks from the baryon. The light-cone helicity amplitudes [42] for wide-angle photoproduction are written as:

$$\begin{aligned} & \mathcal{M}_{0+, \mu+}(\gamma B_1 \rightarrow P B_2) \\ &= \frac{e}{2} \sum_{a,b=u,d,s} \left[\mathcal{H}_{0+, \mu+}^{P(ab)}(s, t) (R_{V, B_1 \rightarrow B_2}^{ab}(t) + R_{A, B_1 \rightarrow B_2}^{ab}(t)) \right. \\ & \quad \left. + \mathcal{H}_{0-, \mu-}^{P(ab)}(s, t) (R_{V, B_1 \rightarrow B_2}^{ab}(t) - R_{A, B_1 \rightarrow B_2}^{ab}(t)) \right], \end{aligned} \quad (2)$$

and

$$\begin{aligned} & \mathcal{M}_{0-, \mu+}(\gamma B_1 \rightarrow P B_2) \\ &= \frac{e}{2} \frac{\sqrt{-t}}{2m} \sum_{a,b=u,d,s} \left[\mathcal{H}_{0+, \mu+}^{P(ab)}(s, t) + \mathcal{H}_{0-, \mu-}^{P(ab)}(s, t) \right] R_{T, B_1 \rightarrow B_2}^{ab}(t), \end{aligned} \quad (3)$$

where μ denotes the helicity of the photon and the helicities of the baryons in \mathcal{M} and of the quarks in the hard scattering amplitude \mathcal{H} are labelled by their signs. H. Huang *et al.* compute the hard scattering amplitudes from the leading order Feynman graphs and the twist-3 pion distribution amplitude. They are expressed in terms of the invariant functions C_i , where C_2 and C_3 provide

the quark helicity non-flip contributions while C_1 and C_4 give the helicity flip contributions,

$$\begin{aligned}
\mathcal{H}_{0+,++}^{P(ab)} &= \sqrt{-\hat{t}/2} \hat{s} \left[C_2^{P(ab)} + C_3^{P(ab)} \right], \\
\mathcal{H}_{0+,-+}^{P(ab)} &= -\sqrt{-\hat{t}/2} \hat{u} \left[C_2^{P(ab)} - C_3^{P(ab)} \right], \\
\mathcal{H}_{0-,++}^{P(ab)} &= -\sqrt{-\hat{u}\hat{s}/2} \left[\hat{t} C_1^{P(ab)} - 2 C_4^{P(ab)} \right], \\
\mathcal{H}_{0-,-+}^{P(ab)} &= \sqrt{-\hat{u}\hat{s}/2} \hat{t} C_1^{P(ab)}.
\end{aligned} \tag{4}$$

While, the form factors $R_{i,B_1 \rightarrow B_2}^{ab}$ represent $1/x$ -moments of GPDs at zero skewness, where $x = \frac{(k_j + k'_j)}{(p + p')}$ is the average momentum fraction the two quarks carry. The form factors parameterize the soft physics that controls the emission and reabsorption of the quarks.

The authors obtain the standard helicity amplitudes, defined in a c.m.s. frame where the photon and the incoming proton move along the 3-direction, via a transform of the light-cone helicity amplitudes, defined in the symmetric frame. In calculating the π^\pm cross sections ratio, the form factors cancel out and if the invariant functions C_1^P and C_4^P are neglected (i.e. neglecting quark helicity flip contributions) and if C_2^P dominates, one obtains [9];

$$\frac{d\sigma(\gamma n \rightarrow \pi^- p)}{d\sigma(\gamma p \rightarrow \pi^+ n)} = \left(\frac{e_u s + e_d u}{e_u u + e_d s} \right)^2. \tag{5}$$

This result coincides with the leading-twist prediction. Fig. 6 indicates that the predicted ratio is

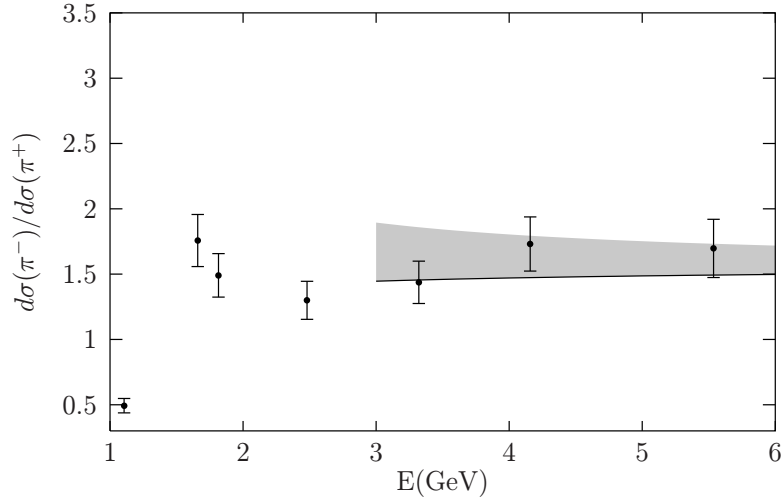


FIG. 6. The ratio of the $\gamma n \rightarrow \pi^- p$ and $\gamma p \rightarrow \pi^+ n$ cross sections versus photon beam energy E , at a c.m.s. scattering angle of 90° . Data are taken from [34]. The solid line is the handbag prediction, with the uncertainties due to target mass corrections [41] indicated by the shaded band.

in surprisingly good agreement with experimental results from JLab [34] given the small photon beam energies ($s_{\text{exp}} = 2mE + m^2$).

On the other hand if the invariant function C_3^P dominates the predicted ratio is [9];

$$\frac{d\sigma(\gamma n \rightarrow \pi^- p)}{d\sigma(\gamma p \rightarrow \pi^+ n)} = \left(\frac{e_u s - e_d u}{e_u u - e_d s} \right)^2, \quad (6)$$

which tends to infinity at large s and a scattering angle of 90° , and is clearly at variance with experiment [34]. For the special case of equal reduced invariant functions, the ratio of cross sections is unity, again in disagreement with data. Thus, there is a strong indication from experiment that the handbag mechanism is at work in these processes with $|C_2^P| \gg |C_3^P|$ under the assumption of negligible quark helicity flip contributions.

The same formalism can be used to obtain the π^0/π^\pm cross section ratios, however, in this case the form factors do not cancel out and a model of the form factors must be used to obtain the ratio. We have obtained such ratios from the authors and they indicate that the contributions from transversity GPDs are small. The predicted π^0/π^\pm cross section ratio at 90° C.M. angle is shown in Fig. 7. However, given the large discrepancy between the different π^0 data sets, it is impossible to compare them to the predictions. This situation points to an urgent need for new measurements using completely different technique compared to the previous experiments that have measured the π^0 cross section at large C.M. angles. The π^0 cross sections measured in this experiment when combined with π^+ cross sections from the G_E^n and G_M^n experiments in Hall A, which will use π^+ photoproduction for calibration, will allow us to extract the π^0/π^+ cross section ratio.

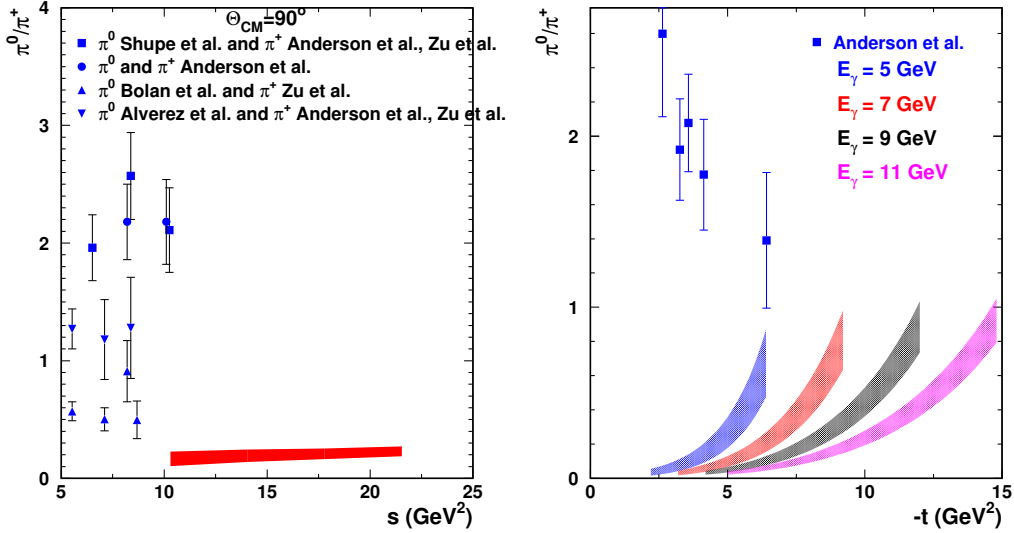


FIG. 7. Left: The π^0/π^+ cross section ratio as a function of \sqrt{s} at a center-of-mass angle of 90° at the highest energies. The red band is the prediction of H. Huang *et al.*[9]. Right: The π^0/π^+ cross section ratio as a function of $|t|$, the bands are predictions of H. Huang *et al.*[9].

The π^0 cross sections, the π^0/π^\pm cross section ratio along with the charged pion ratios will help verify the dominance of the handbag mechanism and/or help identify missing dynamical mechanisms in the handbag approach.

Constituent Counting Rule

The constituent counting rule predicts the energy dependence of the differential cross section at fixed center-of-mass angles for an exclusive two-body reaction at high energy and large momentum transfer as follows:

$$d\sigma/dt = h(\theta_{cm})/s^{n-2}, \quad (7)$$

where s and t are the Mandelstam variables, s is the square of the total energy in the center-of-mass frame and t is the momentum transfer squared in the s channel. The quantity n is the total number of elementary fields in the initial and final states, while $h(\theta_{cm})$ depends on details of the dynamics of the process. In the case of pion photoproduction from a nucleon target, the quark counting rule predicts a s^{-7} scaling behavior for $\frac{d\sigma}{dt}$ at a fixed center-of-mass angle.

The quark counting rule was originally obtained based on dimensional analysis under the assumptions that the only scales in the system are momenta and that composite hadrons can be replaced by point-like constituents. Implicit in these assumptions is the approximation that the class of diagrams, which represent on-shell independent scattering of pairs of constituent quarks (Landshoff diagrams) [43], can be neglected. Also neglected were contributions from quark orbital angular momentum, which are power suppressed but can give rise to hadron helicity flipping amplitudes. These counting rules were also confirmed within the framework of perturbative QCD analysis up to a logarithmic factor of α_s and are believed to be valid at high energy, in the perturbative QCD region. Such analysis relies on the factorization of the exclusive process into a hard scattering amplitude and a soft quark amplitude inside the hadron. It has also been demonstrated that the counting rules for hard exclusive processes can arise from the correspondence between the anti-de Sitter space and conformal field theory [19] which connects superstring theory to superconformal gauge theory.

Many exclusive reactions [13, 32] at high energy and large momentum transfer appear to obey the CCR. A similar trend, i.e. global scaling behavior, has been observed in deuteron photo-disintegration experiments [25–27] and in photo-production of charged pions [34] at a surprisingly low transverse momentum value of ~ 1.1 (GeV/c)². The other natural consequence of pQCD: the helicity conservation selection rule, tends not to agree with data in the experimentally tested region. Hadron helicity conservation arises from quark helicity conservation at high energies and the vector gluon-quark coupling nature of QCD and by neglecting the higher orbital angular momentum states of quarks or gluons in hadrons. The same dimensional analysis which predicts the quark counting rule also predicts hadron helicity conservation for exclusive processes at high energy and large momentum transfers. If hadron helicity conservation holds, the induced polarization of the recoil proton in the unpolarized deuteron photo-disintegration process is expected to be zero. Polarization measurements in deuteron photo-disintegration [28] and π^0 photoproduction [29, 30] have been carried out at JLab. For deuteron photo-disintegration, the induced polarization does seem to approach zero around a photon energy of 1.0 GeV at 90° center-of-mass angle, the polarization transfer data are inconsistent with hadron helicity conservation. The results from π^0 photoproduction are also inconsistent with hadron helicity conservation.

The entire subject is very controversial. Isgur and Llewellyn-Smith [17] argue that if the nucleon wave-function has significant strength at low transverse quark momenta (k_\perp), then the hard gluon exchange (essential to the perturbative approach) which redistributes the transferred momentum among the quarks, is no longer required. The applicability of perturbative techniques at these low momentum transfers is in serious question. There are no definitive answers to the question- *what*

is the energy threshold at which pQCD can be applied? Indeed the exact mechanism governing the observed quark counting rule behavior remains a mystery.

Apart from the early onset of scaling and the disagreement with hadron helicity conservation rule, several other striking phenomena have been observed in pp elastic scattering. One such phenomena is the oscillation of the differential cross-section about the scaling behavior predicted by the quark counting rule (s^{-10} for pp scattering), first pointed out by Hendry [44] in 1973. Secondly, the spin correlation experiment in pp scattering first carried out at Argonne by Crabb *et al.* [45] shows striking behavior: it is ~ 4 times more likely for protons to scatter when their spins are both parallel and normal to the scattering plane than when they are anti-parallel, at the largest momentum transfers ($p_T^2 = 5.09 \text{ (GeV/c)}^2$, $\theta_{c.m.} = 90^\circ$). Later spin-correlation experiments [46] confirm the early observation by Crabb *et al.* [45] and showed that the spin correlation A_{NN} (given by $\frac{\sigma(\uparrow,\uparrow) - \sigma(\uparrow,\downarrow)}{\sigma(\uparrow,\uparrow) + \sigma(\uparrow,\downarrow)}$) varies with energy about the pQCD prediction.

Theoretical interpretation of this oscillatory behavior of the scaled cross-section ($s^{10} \frac{d\sigma}{dt}$) and the striking spin-correlation in pp scattering was attempted by Brodsky, Carlson, and Lipkin [47] within the framework of quantum chromodynamic quark and gluon interactions, where interference between hard pQCD short-distance and long-distance (Landshoff) amplitudes was discussed for the first time. The Landshoff amplitude arises due to multiple independent scattering between quark pairs in different hadrons. Although each scattering process is itself a short distance process, different independent scatterings can be far apart, limited only by the hadron size. Moreover, gluonic radiative corrections give rise to a phase to this amplitude which is calculable in pQCD [48]. This effect is believed to be analogous to the coulomb-nuclear interference that is observed in low-energy charged-particle scattering. It was also shown that at medium energies this phase (and thus the oscillation) is energy dependent [49], while becoming energy independent at asymptotically high energies [49], [50]. Carlson, Chachkhunashvili, and Myhrer [52] have also applied such an interference concept to the pp scattering and have explained the pp polarization data. On the other hand Brodsky and de Teramond [35] have suggested that the structure seen in $s^{10} \frac{d\sigma}{dt}(pp \rightarrow pp)$, the A_{NN} spin correlation at $\sqrt{s} \sim 5 \text{ GeV}$ (around center-of-mass angle of 90°) [45],[46] can be attributed to $c\bar{c}uud\bar{u}ud$ resonant states. The opening of this channel gives rise to an amplitude with a phase shift similar to that predicted for gluonic radiative corrections.

Generalized counting rule

A number of developments have generated renewed interest in this topic. For example, Zhao and Close [53] have argued that a breakdown in the locality of quark-hadron duality (dubbed as “restricted locality” of quark-hadron duality) results in oscillations around the scaling curves predicted by the counting rule. They explain that the smooth behavior of the scaling laws arise due to destructive interference between various intermediate resonance states in exclusive processes at high energies, however at lower energies this cancellation due to destructive interference breaks down locally and gives rise to oscillations about the smooth behavior.

On the other hand, Ji *et al.* [18] have derived a generalized counting rule based on pQCD analysis, by systematically enumerating the Fock components of a hadronic light-cone wave function. Their generalized counting rule for hard exclusive processes include parton orbital angular momentum and hadron helicity flip, thus they provide the scaling behavior of the helicity flipping amplitudes. The interference between the different helicity flip and non-flip amplitudes offers a new mechanism to explain the oscillations in the scaling cross-sections and spin correlations. Brodsky *et al.* [20] have used the anti-de Sitter/Conformal Field Theory correspondence or string/gauge

duality [19] to compute the hadronic light front wave functions exactly and it yields an equivalent generalized counting rule without the use of perturbative theory. In a further test of these approaches, calculations of the nucleon form factors including quark orbital angular momentum in pQCD [54] and those computed from light-front hadron dynamics [20] both seem to explain the $\frac{1}{Q^2}$ fall-off of the proton form factor ratio, $G_E(Q^2)/G_M(Q^2)$, measured at JLab in polarization transfer experiments [55].

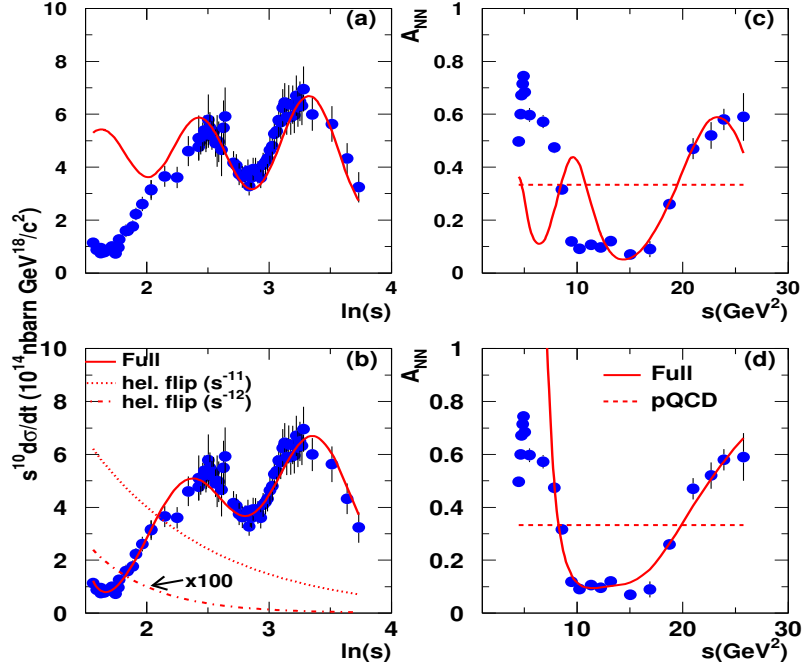


FIG. 8. (a) The fit to pp scattering data at $\theta_{cm} = 90^\circ$ of Ralston and Pire [51]. (b) Fit The same data when the helicity flipping amplitudes are included. The solid line is the fit result, the dotted line is contribution from the helicity flip term $\sim s^{-11}$, the dot-dashed line is contribution from the helicity flip term $\sim s^{-12}$. The $\sim s^{-12}$ contribution has been multiplied by 100 for display purposes. (c) The fit to A_{NN} from polarized pp scattering data at $\theta_{cm} = 90^\circ$ of Carlson *et al.* [52]. (d) Fit to the same data when the helicity flip amplitudes are included. The cross-section data are from Ref. [57] and the A_{NN} data are from Ref. [45, 46].

We examined [56] the role of the helicity flipping amplitudes in the oscillatory scaling behavior of pp scattering and the oscillations in the spin correlations observed in polarized pp scattering. We noticed that just using the Landshoff amplitude and its interference with the short distance term, fails to describe the data at low energies ($s < 10 \text{ GeV}^2$). Since the Landshoff amplitude is expected to be significant only at high energies, it is not unreasonable that the above formalism does not describe the data at low energies. We used the generalized counting rule of Ji *et al.* [18] to obtain the scaling behavior of the helicity flipping amplitudes. Our fit [56] including the helicity flip amplitudes describes the scaled cross-section as well as the spin-correlation data much better

especially at the low energies (Fig. 8). The helicity flip amplitudes arising from the parton orbital angular momentum are non-negligible when the parton transverse momentum can not be neglected compared with the typical momentum scale in the exclusive processes. At relatively low energies this is certainly the case, and thus one would expect the helicity flip amplitudes to be a significant contribution to the cross-section at low energies. Moreover, the generalized counting rule of Ji *et al.* predicts a much faster fall-off with energy for the helicity flip amplitudes as expected. An examination of the explicit contribution from the different amplitudes show that the helicity flip amplitudes and their interference are indeed quite significant at low energies and help describe the data at low energies. Results from our fits are shown in Fig. 8. These are very promising results and should be examined for other reactions.

Is oscillatory scaling behavior unique to proton-proton elastic scattering?

It was previously thought that the oscillatory $s^{10} \frac{d\sigma}{dt}$ feature is unique to pp scattering or to hadron induced exclusive processes. However, it has been suggested that similar oscillations should occur in deuteron photo-disintegration [58], and photo-pion productions at large angles [59]. The QCD re-scattering calculation of the deuteron photo-disintegration process by Frankfurt, Miller, Sargsian and Strikman [58] predicts that the additional energy dependence of the differential cross-section, beyond the $s^{11} \frac{d\sigma}{dt}$ scaling arises primarily from the $n - p$ scattering in the final state. If these predictions are correct, such oscillatory behavior may be a general feature of high energy exclusive photoreactions. Thus it is very important to experimentally search for these oscillations in photoreactions.

Farrar, Sterman and Zhang [60] have shown that the Landshoff contributions are suppressed at leading-order in large-angle photoproduction but they can contribute at subleading order in $\frac{1}{Q}$ as pointed out by the same authors. In principle, the fluctuation of a photon into a $q\bar{q}$ in the initial state can also contribute an independent scattering amplitude at sub-leading order. However, the vector-meson dominance diffractive mechanism is already suppressed in vector meson photoproduction at large values of t [61]. On the other hand such independent scattering amplitude can contribute in the final state if more than one hadron exist in the final state, which is the case for both the deuteron photo-disintegration and nucleon photo-pion production reactions. Thus, an unambiguous observation of such an oscillatory behavior in exclusive photoreactions with hadrons in the final state at large t may provide a signature of QCD final state interaction. The later data on $d(\gamma, p)n$ reaction [26, 27] show that the oscillations, if present, are very weak in this process, and the rapid drop of the cross section ($\frac{d\sigma}{dt} \propto \frac{1}{s^{11}}$) makes it impractical to investigate such oscillatory behavior.

Given that the nucleon photo-pion production has a much larger cross-section at high energies ($\frac{d\sigma}{dt} \propto \frac{1}{s^7}$), it is very desirable to use these reactions to verify the existence of such oscillations. Some precision data on $\gamma p \rightarrow \pi^+ n$ and $\gamma n \rightarrow \pi^- p$ has been reported by JLab two experiments [34, 37]. The results indicate the constituent counting rule behavior at center-of-mass angle of 90° , for photon energies above ~ 3 GeV (i.e. above the resonance region) [34]. The $\gamma n \rightarrow \pi^- p$ data [37] also confirm a broad enhancement, followed by a rapid falloff, in the scaled differential cross section $s^7 \frac{d\sigma}{dt}$ around a c. m. energy, $\sqrt{s} = 2.1$ GeV at center-of-mass angle of 90° . There is also an angular dependence of this enhancement as the scaling region is approached for $\theta_{c.m.}$ from 70° to 105° . The world data suggest a similar trend for the π^0 photoproduction process, however, the data at the highest energies are inconsistent and do not extend to as high an energy as for the charged pion photoproduction.

In addition to the s^{-7} scaling behavior, the JLab data [34] also suggest an oscillatory behavior. However, the rather coarse beam energy settings prevent a conclusive statement about the oscillatory behavior. The photo-pion production data can be described, as in case of pp scattering, by including the helicity flip terms along with the Landshoff terms [56], however, because of the coarse energy spacing of the data the results of these fits are not as illustrative.

As mentioned earlier, the π^0 photoproduction is one of the few exclusive processes where the scaling behavior has not been verified and there is a lack of consistent data at high values of Mandelstam variables (s , t and u). Thus, to verify any structure in the scaled cross-section of photo-pion production processes and to understand its origin, it is imperative that we do a scan of the scaling region for the $\gamma p \rightarrow \pi^0 p$ processes and extend measurements to much higher center-of-mass energies over a range of center-of-mass angles. A energy scan of the charged pion photoproduction would require multiple energy changes which is not readily available, however, for neutral pions when using a high resolution (position and energy) calorimeter one can scan over larger energy range with fewer energy changes.

Summary of motivations

The π^0 cross sections and cross section ratios (formed by combining data from this proposal with those from other Hall-A experiments) at wide angles and large momentum transfer will provide tests of the dominance of handbag mechanism. They will also help identify any missing dynamical mechanism in the handbag approach.

The π^0 cross sections will help study the details of the energy and angular dependence of the scaling and help understand the exact mechanism behind the relatively early onset of scaling. It will also help investigate the details of the agreement with scaling laws and provide insight into any oscillations about the scaling behavior.

All of these results will help identify the energy scale for the transition from the soft to hard factorization regimes and help understand the non-perturbative structure of the proton.

THE PROPOSED MEASUREMENT

We propose to carry out a measurement of the photo-pion production cross-section for the fundamental process $\gamma p \rightarrow \pi^0 p$ on a liquid hydrogen target over a pion center-of-mass angle ranging between $55^\circ < \theta_{CM} < 105^\circ$, and \sqrt{s} over a range of $E_\gamma \sim 6$ GeV to 10 GeV. The π^0 photoproduction is the dominant background for the WACS experiment. Thus we propose to use the same setup as the WACS experiment and extract the π^0 cross section from the same data which is collected during the WACS experiment. The recoil protons will be detected in the High-Momentum Spectrometer (HMS) in standard configuration. The photons from the π^0 decay will be detected by the Neutral Particle Spectrometer (see Fig. 9). All of the key equipment is described in the following sections.

The CEBAF Electron Beam

The maximum electron beam energy required is 11 GeV, in addition beam energies of 8.8 GeV and 6.6 GeV are also required. An unpolarized beam with currents up to 60 μ A will be used on a

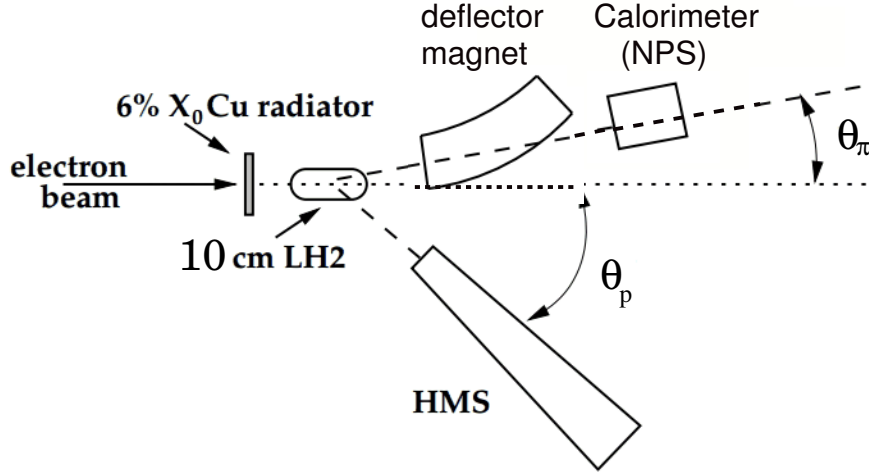


FIG. 9. Schematic of the experimental setup

10 cm long liquid hydrogen target. This implies an average luminosity of $\mathcal{L}_{ep} = 1.6 \times 10^{38}/\text{cm}^2/\text{s}$.

Target and Radiator

The experiment will utilize one of the standard Hall C liquid hydrogen (LH2) targets with a 10 cm-long machined cell with aluminum walls of 5 mm thickness, which has been successfully employed in many experiments at JLab. The copper radiator with a thickness of $t_{rad}/X_0 = 0.06$ (6% of radiation length) will be mounted on the cell block about 25 cm upstream of the cell entrance window. The distance between the target and the radiator and the high photon energies help avoid the background produced on the walls of the target and keeps the photon beam spot compact, which allows both accurate measurement of the proton momentum with the vertical bend spectrometer and operation with high luminosity. Further, the distance between the radiator and the target allows additional shielding to be installed to reduce the scattering from the radiator. Note that in the rate simulations described later in the proposal, the effective thickness of the radiator was assumed to be slightly larger, $t_{rad}/X_0 = 0.08$, due to additional radiative processes in the target and the virtual photon flux.

Deflection Magnet

Previous RCS experiments have shown that a deflection magnet provides an effective way to discriminate between elastic electron and photon scattering events. When a deflection magnet is used there is no need for a veto detector, which in turn allows for at least ten times higher

photon/electron beam intensity. The deflection magnet for the new WACS experiment has been designed with the following considerations:

- Aperture for the full size of the calorimeter;
- Value of the magnetic field for electron deflection;
- Minimum magnetic field at the beam line;
- Horizontal orientation of the magnetic field.

Additional information about the magnet design is presented in Ref. [11].

One of the key aspects in discriminating the signal from background, in both the WACS and photopion experiments, is a reliable comparison of the expected and measured electron-proton (calorimeter-HMS) correlation. The angular spread of this correlation is smaller out-of-plane because it is defined only by angular resolution; in contrast, it is larger in-plane because its dominant contribution comes from the proton momentum reconstruction resolution for a given proton momentum. Typically the out-of-plane resolution relevant for the e-p correlation is twice as good as the in-plane resolution. The bending direction for elastic electrons should therefore be vertical (magnetic field horizontal) in order to minimize the required deflection of electrons and the resulting value of the field in the deflection magnet.

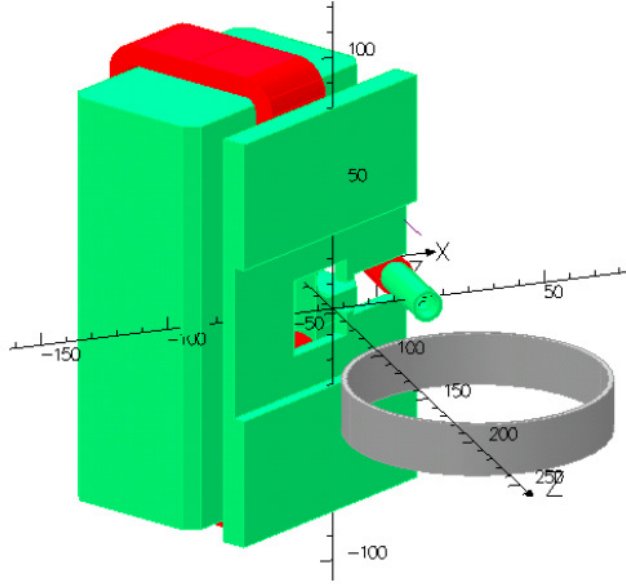


FIG. 10. An image of the deflection magnet for the WACS experiment from the TOSCA analysis package, with the magnet placed at a 30 degree scattering angle with 110 cm between the magnet center and the target.

In order to extract the π^0 cross section the shape of the pion related events need to be well understood. The deflector magnet must therefore relocate the electrons sufficiently far from the π^0 decay events. This can be accomplished by a sufficiently strong deflector magnet. A magnet that will be able to provide a field integral of up to $\int B \cdot dl \sim 0.6 Tm$ has been designed and will be

constructed for the proposed WACS experiment. It will be placed as shown in Fig. 9 and an image of the magnet is shown in Fig. 10. We will use the same magnet for the additional kinematics covered in this proposal.

The High Momentum Spectrometer

The recoil protons in the proposed experiment will be detected by the High-Momentum Spectrometer (HMS), which is part of the standard equipment of Hall C. The HMS is a high resolution ($\delta p/p < 10^3$) magnetic spectrometer in a QQD magnet configuration with a maximum momentum of 7.5 GeV/c and a momentum bite of 18 %. It has an octagonal input aperture with an effective solid angle coverage of approximately 6 msr and can be positioned to angles greater than 12.5° . The detector package of the HMS consists of two vertical drift chamber packages for track reconstruction, scintillator hodoscopes for timing, as well as a gas Čerenkov counter, an aerogel Čerenkov counter, and a segmented lead-glass shower calorimeter for particle identification. If needed, the shower calorimeter could be used in the trigger. The HMS can be tuned in parallel-to-point mode (for optimal in-plane angle accuracy) or point-to-point mode (for best vertex reconstruction). In the proposed experiment it will be used in the latter mode in which extended targets can be accommodated with a vertex reconstruction accuracy of 1 mm, and where both in-plane and out-of-plane angle measurement resolutions are about 0.8 mrad. In this proposal the SIMC simulation package was used for determination of the actual momentum and angular resolutions, which included scattering in the target material as well as reconstruction effects. The simulation is further elaborated in a later section.

Expected Rates

The DINREG Monte Carlo code developed by the RadCon group at JLab [?] has been used to calculate the expected proton and π^+ rates in the HMS for each of the proposed kinematic settings. Fig. 11 shows the simulated HMS singles rates, and the simulated proton-to- π^+ ratio.[updated figure with 6.6 GeV points is awaiting simulation]. The maximum HMS singles rate is at point xy and is around xy kHz. The equivalent trigger rate (for protons only) for this same kinematic point is xy kHz. These rates are well within the capabilities of the HMS.

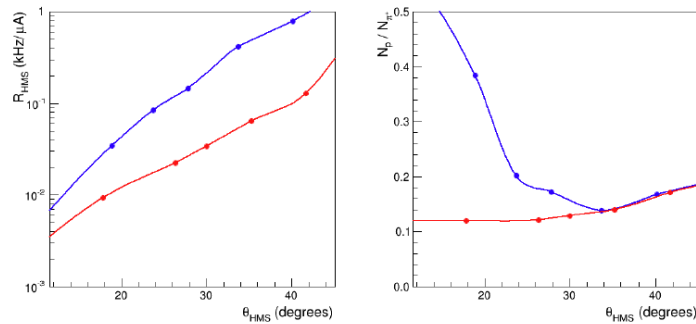


FIG. 11. Simulated raw singles rates in the HMS (left) and proton-to- π^+ ratio (right)

The Photon Calorimeter

The photon calorimeter for this experiment will be the new Neutral Pion Spectrometer [10] being proposed for Hall-C. This photon calorimeter will consist of a rectangular array of 31 (horz) \times 36 (vert) PbWO_4 crystal blocks with dimensions $2.05 \times 2.05 \times 18 \text{ cm}^3$. Each crystal is attached to a photomultiplier tube and base. The proposed calorimeter is based on the existing HYCAL calorimeter [63]. Fig. 12 shows an array of crystal blocks that will closely resemble the one that will be used in the proposed experiment.

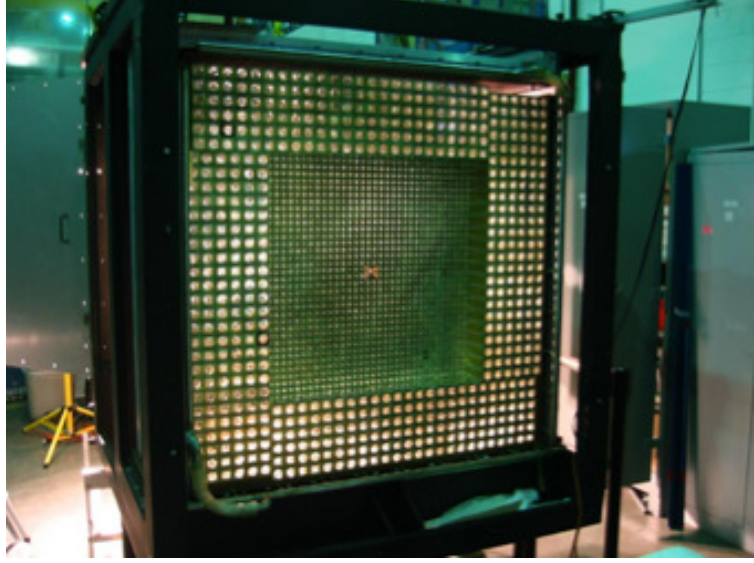


FIG. 12. The central high-resolution PbWO_4 part of the HYCAL detector will be used in the NPS.

The PMTs are shielded from ambient light in a light-tight box that contains an aircooling system, whose main purpose is to prevent the PMTs from overheating and aid in the overall stable operation of the calorimeter. The yield of the PbWO_4 crystals is temperature dependent, with $\approx 2\%/^{\circ}\text{C}$ deterioration of light yield around room temperature. HV and signal-cable systems are also contained in the light box encasing the PMTs. The calorimeter will be equipped with a system that distributes light pulses to each calorimeter module. The main purpose of this system is to provide a quick way to check the detector operation and to calibrate the dependence of the signal amplitudes on the applied HV. The detector response to photons of a given energy may drift with time, due to drifts in the PMT gains and to changes in the glass transparency caused by radiation damage. For this reason, the gain monitoring system will also allow measurements of the relative gains of all detector channels during the experiment. The calorimeter can be moved into the hall without being disconnected from the frontend electronics, which is located in racks a few feet behind the main detector components. The position of the photon arm will be adjusted for each kinematics to match the angular position of the HMS. The calorimeter will most likely be placed on rails and repositioned by sliding along these rails. To shield from radiation it will be very beneficial to place a 10 cm thick plastic cover with an effective surface area thickness of approximately $10\text{g}/\text{cm}^2$ in front of the calorimeter.

Expected Rates

DINREG Monte Carlo simulations for the expected NPS singles rates have also been performed for each of the proposed kinematic points [?]. The total number of γ, e^+ and e^- incident on the calorimeter with energy greater than 1 GeV gives a maximum singles rate of xy MHz. The simulated rates are shown in Fig. 13.[figure with 6.6 GeV points is awaing simulation].

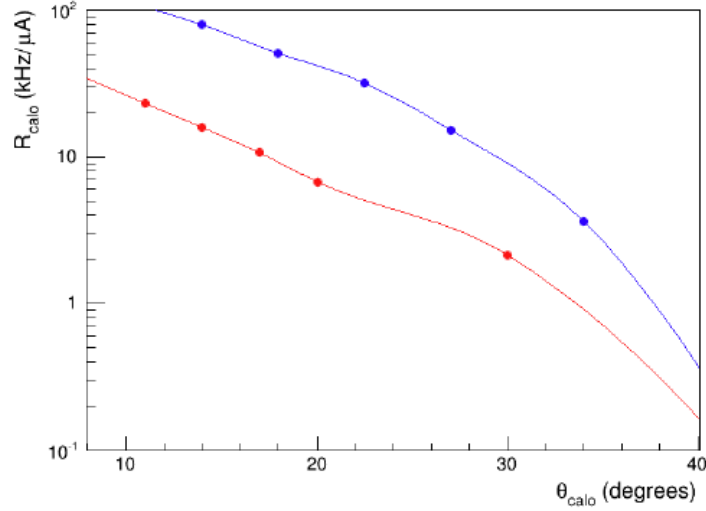


FIG. 13. Simulated raw singles rates in the NPS

Trigger and DAQ

The HMS trigger will be the only trigger for this experiment, this is possible because of the modest event rate expected in the proton arm at high photon beam energies and because the new HMS and NPS pipeline based electronics will be dead-time free. Hence each particle detected by the HMS will trigger the DAQ readout of both the HMS and the calorimeter. The cluster summing trigger for the calorimeter will not be implemented. The read-out of the NPS FADCs will be controlled by FPGA based hardware, which will be programmed to recognise where a hit has occurred and will read out only the relevant group of FADC modules. This will avoid generation of extraneous data.

The typical NPS event size is expected to be 1 kB, while the HMS event size is expected to be less than 2 kB [11]. Since the trigger will be formed by the HMS, the maximum data throughput will be at kinematic point xy where, the expected trigger rate is xy kHz. These numbers, along with the expected NPS singles rates gives the a maximum DAQ rate of ~ 2 MB/s and a total dataset of around 1 TB. Both these numbers are well within the capabilities of the online DAQ and data storage facilities.

Radiation Budget

The high luminosity required in the proposed experiment could result in loss of the energy and coordinate resolutions of the calorimeter due to pileup. Long operation at high radiation load could cause radiation damage to the crystals and loss of their performance.

In order to estimate the potential for radiation damage to the calorimeter crystals, the DIN-REG simulation code was used. The total dose rate incident upon the NPS calorimeter for each kinematic point and the proposed running conditions has been calculated, with the results shown in Fig. 14.[figure with 6.6 GeV points to come soon] The maximum expected rate is xy krem/h for kinematic point xy. Assuming the dose is deposited over the full crystal length, this simulation gives a total accumulated dose estimate for the full beam-time of xy kRad. This does not include the effects of shielding the calorimeter from low energy electromagnetic radiation, with shielding the radiation dose is expected to be xy krad. Although these numbers are significant, they are still more than acceptable according to a study [65], which found that at a value of 1 Mrad, the light output reduction for $PbWO_4$ is around 2%.

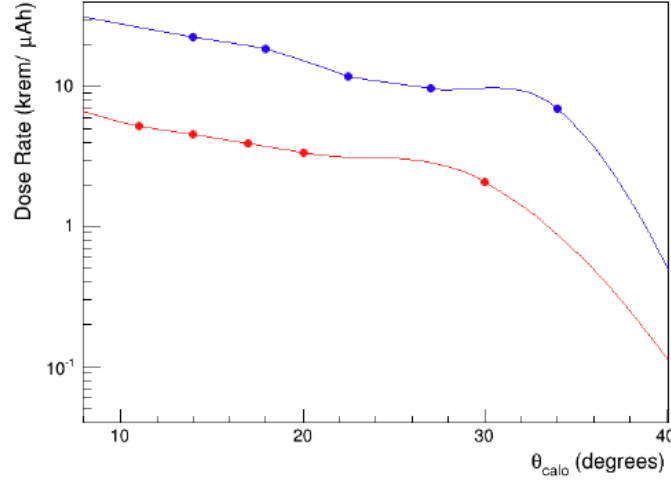


FIG. 14. Simulated radiation dose in the NPS

Using the data from the previous RCS experiment in 2002, the radiation level in Hall C during the proposed experiment is expected to be of the order of 200 mR/hour. The radiation load could be reduced by a factor of 2, if necessary, by using modest local shielding of the radiator and the target installed at angles above 50°.

Energy and Coordinate Resolution

The energy of the particle detected in the calorimeter is calculated from a sum of the signals in several crystals (up to 9) which form a cluster. The noise in the ADC used for a measurement of the signal from an individual crystal contributes to the detector energy resolution. In a high-

rate experiment the ADC noise is increased, and this can be characterized by the ADC pedestal width. Using the observed 5-6 MeV pedestal width observed in the previous RCS experiment, the expected pedestal width for the this proposal is projected to be around 50 MeV. The effect of the background on the energy resolution could be estimated from this estimated pedestal width and the number of modules in the cluster. It is expected to be on the level of 110-150 MeV or 3.3-4.5%, a similar estimate shows that the effect on the coordinate resolution is around 0.5 mm.

Kinematic settings

The differential cross section for Wide-angle π^0 photoproduction will be determined at photon energies of 5.0 - 11.0 GeV at $70^\circ < \theta_{CM} < 110^\circ$. The kinematic for two standard beam energies of 8.8 GeV and 11 GeV is exactly the same as those for the new proposed RCS experiment. These kinematics are shown in Table I. The coverage in $|t|$ and s for these two beam energies is shown in Fig. 15 (right panel). However, unlike the RCS experiment we want to measure the cross section at a third standard beam energy of 6.6 GeV. The $|t|$ and s coverage for this beam energy is shown separately in Fig. 15 (left panel). The kinematics for 6.6 GeV beam is shown in Table II. In all cases, the scattering angles and momenta fall well within the allowed range for the HMS and the NPS and pose no practical difficulties in terms of positioning of the detector systems.

TABLE I. Table of kinematics for the $p(\gamma, \pi^0 p)$ reaction for E_{beam} of 8.8 and 11 GeV. These are identical to the WACS proposal and will be collected as part of the background to the WACS experiment.

	E_γ	θ_{CM}^π	\sqrt{s}	$ t $	θ_p (lab)	θ_{π^0} (lab)	P_p	P_{π^0}
4A	8.0	55.8	3.99	3.10	40.1	14.2	2.416	6.347
4B	8.0	67.6	3.99	4.39	33.7	17.9	3.138	5.663
4C	8.0	80.4	3.99	5.91	27.8	22.5	3.978	4.851
4D	8.0	90.9	3.99	7.20	23.7	26.9	4.684	4.161
4E	8.0	104.8	3.99	8.90	18.9	34.0	5.605	3.255
5A	10.0	48.9	4.43	3.07	41.7	11.0	2.399	8.362
5B	10.0	59.5	4.43	4.41	35.3	13.8	3.154	7.647
5C	10.0	70.1	4.43	5.91	30.0	16.9	3.981	6.848
5D	10.0	78.7	4.43	7.21	26.3	19.7	4.687	6.158
5E	10.0	103.2	4.43	11.01	17.8	29.9	6.739	4.135

TABLE II. Table of kinematics for the $p(\gamma, \pi^0 p)$ reaction at E_{beam} of 6.6 GeV at pion C.M. angle of 55, 70, 90 and 105°.

	E_γ	θ_{CM}^π	\sqrt{s}	$ t $	θ_p (lab)	θ_{π^0} (lab)	P_p	P_{π^0}
3A	6.0	55	3.48	1.86	43.9	15.9	1.904	4.814
3B	6.0	70	3.48	3.44	35.6	21.2	2.602	4.170
3C	6.0	90	3.48	5.21	26.7	30.1	3.595	3.218
3D	6.0	105	3.48	6.98	21.1	38.5	4.334	2.50

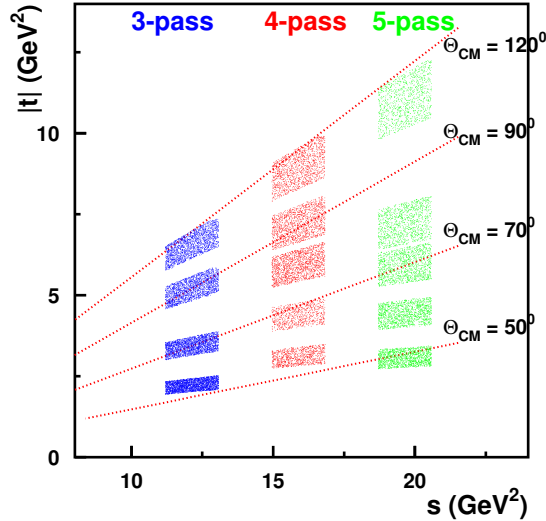


FIG. 15. Kinematic coverage with the 3 pass, 4 pass and 5 pass beams.

Monte Carlo Simulation

The RCS collaboration has developed a Monte Carlo simulation in order to study the feasibility of extracting the RCS signal from large backgrounds due to the π^0 decay and elastic e - p scattering. Events are first generated over a much broader kinematic range compared to the detector acceptances, according to cross section parameterizations of the three reaction types: RCS, neutral pion photoproduction, and elastic ep scattering. In order to study the feasibility of extracting the photoproduced π^0 , we have added two more reactions 2-pion production and η production. The parameterizations of the cross sections are based on E99-114 data in the case of RCS and neutral pion photoproduction [66] and the Bosted fit to the Sachs form factors for elastic ep scattering events [67]. The 2-pion and η production cross sections were obtained from the Durham database [68]. The proton interactions in the target and HMS are then simulated using the standard Hall C SIMC simulation package, while the particles scattered towards the NPS (photons, pions and electrons) are simulated using dedicated software developed within the CERN Geant4 framework. This latter tool includes a realistic simulation of the target, scattering chamber, deflection magnet and the NPS. The technique developed and refined for identifying RCS events and extracting the associated yield, namely, one assumes two-body kinematics and uses the measured recoil proton variables to reconstruct a predicted hit position for the corresponding scattered photon at the NPS. The differences between the predicted and measured NPS hit positions, δx and

δy , are then used to identify the reaction from which a particular event originated. The same technique was found to work very well in distinguishing 1-pion from 2-pion events. Above the η production threshold, the η events are distinguishable from the 1-pion events, however the η production rates were negligible compared to the 1-pion rates.

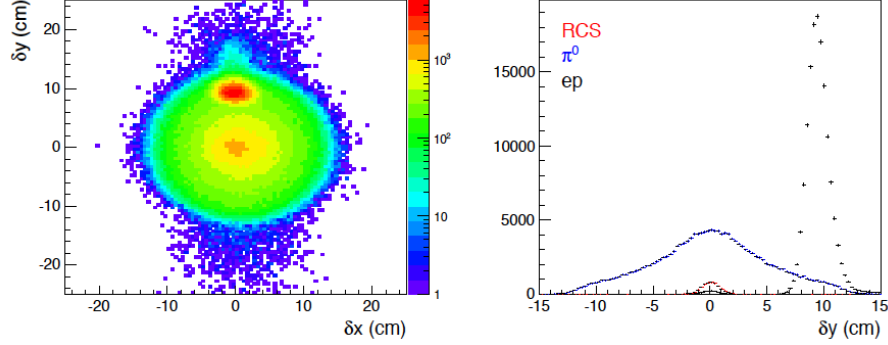


FIG. 16. Typical NPS hit difference distributions for kinematic point 4D. (Left) δx vs δy for all events. (Right) A projection on to δy for events in the central δx region.

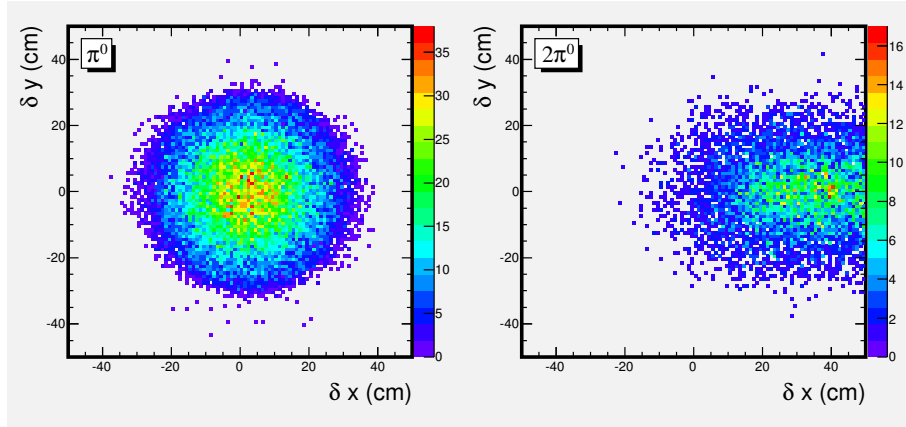


FIG. 17. (Left) δx vs δy for π^0 events for kinematic point 3B. (Right) δx vs δy for $2\pi^0$ events.

The distributions shown in Figs. 16, 17 and 18 correspond to the difference between the expected NPS hit positions for a good proton track in the HMS and the center-of-gravity positions of the highest energy NPS cluster. In Fig. 16 one can see that the elastic ep events are centered at positive δy due to deflection in the magnet, RCS events are centered around zero, and events from detection of one of the photons from the decay of a neutral pion form a relatively broad background. In Fig. 17 we compare the δx and δy for single pion (left) and two pion (right) events. The photons from the decay of 2-pion events have relatively large δx and δy , and once a cut corresponding to $\pm 1.5\sigma_x$ (where σ_x is the x-resolution of the calorimeter) is applied, very few of the 2-pion events end up being wrongly identified as 1-pion events, as seen in Fig. 18.

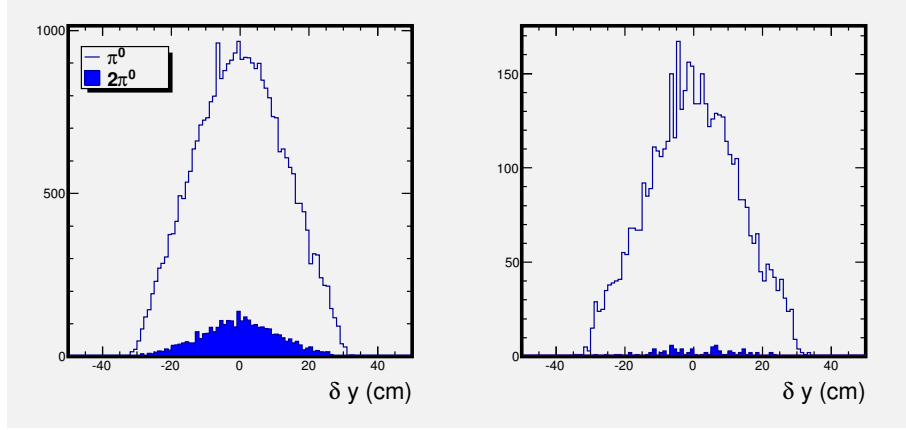


FIG. 18. Left: A projection on to δy for all π^0 and $2\pi^0$ events (red). Right: A projection on to δy for π^0 and $2\pi^0$ events (red) in the central δx region.

The free parameters associated with the experimental set-up i.e. the deflection magnet distance and field integral, as well as the NPS distance have been optimized with the Monte Carlo simulation for all kinematic settings in order to maximize the deflection of the electrons from ep events, minimize the resolution of the NPS hit difference distributions as well as the relative number of background events compared to the signal. The optimized values of the parameters of the experimental settings are shown in Tables III and IV.

Another interesting feature of this experiment will involve the dual role for the events close to the end point of the Bremsstrahlung spectrum which is well below the two pion threshold. For these π^0 events there are no 2-pion or η backgrounds. Therefore, these events can also be used to optimize and then monitor the π^0 acceptance and efficiency of the calorimeter. The measured π^0 acceptance function can then be used to build better simulations of the calorimeter.

Physics Background

Although the deflection magnet deflects the ep elastic events away from the RCS peak it does not deflect it completely outside the NPS acceptance. Thus the ep events are the dominant background for the extraction of the π^0 yield. The ratio N_{ep}/N_{π^0} varies between xx - yy, while the N_{RCS}/N_{π^0} varies between xx -yy. Experience from previous JLab WCS experiments has shown that good calorimeter energy resolution, two-cluster analysis along with a Monte Carlo simulation can be used to fit the pion, the RCS and the ep events and extract the pion yield. For this reason, one other critical factor in the final values chosen for the NPS distance has been to ensure that the distribution of pion events in δx and δy is not artificially truncated by the NPS acceptance. The ratio $N_{2\pi^0}/N_{\pi^0}$ and N_{η}/N_{π^0} varies between xx -yy in the in the $1.5\sigma_x$ central $\delta x - \delta y$ region. These cannot be separated from the single pion events and will lead to a systematic uncertainty. Contribution from these events will be corrected for using an estimate from a Monte Carlo simulation.

Detector Resolution

Based on the experience from previous JLab WACS experiments, it has been established that the two-arm resolution for the calorimeter hit difference distributions, is dominated by i) proton multiple scattering and reconstruction in the proton spectrometer, and ii) the out-of-plane (δy) resolution is much better than the in-plane (δx) resolution, as a result of the fact that the latter includes significant contributions from the proton momentum and vertex resolutions. This is the primary reason that a horizontal magnetic field, and therefore vertical deflection, is critical to the success of the proposed measurements. Typical values for the expected NPS position and energy resolutions have been included in the Monte Carlo simulation, as have photon/electron interactions in the target, scattering chamber and a 10-cm plastic shield directly in front of the NPS which acts as a shield from low energy electromagnetic background. These result in a contribution to the resolution over all kinematic settings of around 0.35 cm. For the range of proton momenta considered in the present proposal (1.791 - 7.586 GeV/c), the in-plane angular resolution varies between 1.5 and 2.5 mrad, the out-of-plane resolution between 1.7 and 3.8 mrad, and the $\delta p/p$ resolution between 5 and 7.5×10^4 . It is primarily the last (although there is a small contribution from the vertex resolution) that leads to the δx resolution being poorer than the δy resolution. The NPS distance clearly plays a crucial role in determining the final values for the two-arm resolutions. It has therefore been optimized for all kinematic settings such that the out-of-plane resolution remains around or less than 1 cm at the two highest beam energies and less than 2 cm for the setting using the 6.6 GeV beam.

TABLE III. Table of parameters for the experimental setup for the $E_{\text{beam}} = 8.8$ and 11 GeV settings. These are exactly the same as the settings for the RCS experiment.

Label	D_{NPS} (m)	D_{mag} (m)	$\int B \cdot dl$ (Tm)	σ_x (cm)	σ_y (cm)	e-defl (cm)	$N_{ep\gamma}/N_{\pi^0}$	$N_{\pi^0\pi^0}/N_{\pi^0}$	N_{η}/N_{π^0}	N_{RCS}/N_{π^0}
-------	------------------	------------------	---------------------------	--------------------	--------------------	----------------	--------------------------	----------------------------	----------------------	---------------------

TABLE IV. Table of parameters for the experimental setup for the E_{beam} of 6.6 GeV settings.

Label	D_{NPS} (m)	D_{mag} (m)	$\int B \cdot dl$ (Tm)	σ_x (cm)	σ_y (cm)	e-defl (cm)	$N_{ep\gamma}/N_{\pi^0}$	$N_{\pi^0\pi^0}/N_{\pi^0}$	N_{η}/N_{π^0}	N_{RCS}/N_{π^0}
3A 3B 3C	7.0	1.1	0.6	2.66	1.21	10.9	0.11	0.01	2.0×10^{-4}	0.19

Rates and Systematic Uncertainties

The expected RCS event rate for the kinematic settings given in Tables 2 has been calculated with the Monte Carlo simulation and yield extraction analysis technique described above. The event rate is the product of the luminosity, the cross section, and the acceptances of the detectors, as well as all other factors such as DAQ dead time, efficiency of the trigger, and the detectors and

efficiency of the reconstruction analysis. The rate was calculated as:

$$N_{\pi^0} = \frac{d\sigma}{dt} \frac{(E_\gamma^f)^2}{\pi} \Delta\Omega_\gamma f_{\gamma p} \left(\frac{\Delta E_\gamma^f t_{rad}}{E_\gamma^f X_0} \right) \mathcal{L}_{ep},$$

where $\frac{d\sigma}{dt}$ is the photopion cross section, the factor $\frac{(E_\gamma^f)^2}{\pi} \Delta\Omega_\gamma$ is the range of Δt for a given kinematics, $f_{\gamma p}$ is the fraction of events detected for a given range of photon energies E_γ^f , $\frac{\Delta E_\gamma^f t_{rad}}{E_\gamma^f X_0}$ is the photon flux, i.e. the number of photons produced per incident electron (including photons produced in the target and virtual photons), and \mathcal{L}_{ep} is the electron-proton luminosity.

The raw singles rates in the HMS and NPS have been determined for events arising from RCS, elastic ep scattering and π^0 photoproduction. The HMS singles rates for π^+ photoproduction have also been calculated. These are shown for a corresponding electron beam current chosen for each kinematic setting in Tables V and VI. For all settings the HMS trigger rate will be well within acceptable HMS operating parameters as determined in previous HMS experiments. The π^+ rates are such that rejection of these events off-line via the kinematic reconstruction technique described in previous sections will be sufficient, without the need for any additional particle identification.

TABLE V. Table of rates for the $E_{beam} = 8.8$ and 11 GeV settings. These are exactly the same as the settings for the RCS experiment.

Label	I_{beam} (μA)	R_{HMS}^p (Hz)	$R_{HMS}^{\pi^+}$ (Hz)	R_e (Hz)	R_γ (Hz)
-------	---------------------------	---------------------	---------------------------	---------------	--------------------

TABLE VI. Table of rates for the E_{beam} of 6.6 GeV settings.

Label	I_{beam} (μA)	R_{HMS}^p (Hz)	$R_{HMS}^{\pi^+}$ (Hz)	R_e (Hz)	R_γ (Hz)
3A					
3B					
3C					
3D					

The three main sources of systematic uncertainties in the proposed measurement of the π^0 cross section are those associated with the yield extraction, the determination of the detector acceptance and efficiencies, and the determination of the total photon beam flux. As before, extensive experience gained during the E99-114 and E07-002 experiments in combination with the Monte Carlo simulation studies detailed in the previous section is relied upon to make estimates of these various sources of systematic uncertainties. Adding the various contributions described below in quadrature, it is estimated that the total systematic uncertainty for the proposed measurement will be around 8% for the least favorable kinematic setting. Beginning with the total photon beam flux, there are contributions to this particular uncertainty from measurement of the accumulated electron beam charge, target thickness, and determination of the bremsstrahlung photon flux for a given energy range. This last dominates, while the others are estimated to be less than 1%. The utilization of redundant calculations of the bremsstrahlung flux (using both Geant4 and dedicated thick-target bremsstrahlung tools) and measurements using the actual data lead to confidence that

this uncertainty can be kept around the 3% level. Furthermore, previous experience working with the HMS, the simple geometry of the NPS, and the fact that the HMS will be operating well within its capabilities lead to the expectation that the systematic uncertainty associated with detector acceptances and efficiencies will be around the same 3% level. The extraction of the π^0 yield will have uncertainties from the RCS, ep , 2π and η backgrounds, which vary relative to each other for different kinematic settings. In order to estimate the magnitude of the systematic errors arising as a result of contamination from these background sources (as given by the ratios in Table. III, and IV), we have relied on the analysis of the RCS collaboration. Since the 2π and η contaminations are small, the major contributions to the uncertainty are from the ep and RCS contaminations and are therefore same as those for the RCS experiment. Based on the Monte Carlo simulations an additional 1% uncertainty is assigned due to background from 2π and η .

Beam Time Request

The beam-time request is based on the time to achieve a combined uncertainty of 10% (2% statistical). These numbers have been calculated based on the expected rates given in the previous section and include estimated overheads from sources such as accelerator downtime, DAQ dead-time, detector inefficiencies and configuration changes between kinematic settings. In total, the beam-time estimate for the 4-pass kinematic settings and 5-pass settings are exactly same those for the RCS experiment, since the π^0 data will be collected at the same time as the RCS experiment. The additional beam-time needed for the 3-pass running is xy hours over the 3 different settings as shown in Table VII, and VIII.

TABLE VII. Beamtime request for the E_{beam} of 8.8 and 11 GeV settings.

Projected Results

The π^0 photoproduction cross sections measured in this experiment will cover a large range of C.M. energy overlapping with previous measurements at $s < 10\text{GeV}^2$, and extending up $s \sim 20\text{GeV}^2$. These results may help resolve the discrepancy between the previous measurements. Fig. 19 shows the projected results at 90° C.M. angle.

The G_E^n and G_M^n Experiments in Hall-A using the SBS and Big-Hand spectrometers will use π^+ photoproduction for calibration. When combined with the proposed π^0 photoproduction of this experiment, one can extract π^0/π^+ ratios to compare with models that have successfully described Compton scattering data. These results can help verify the dominance of the handbag mechanism.

TABLE VIII. Beamtime request for the E_{beam} of 6.6 GeV settings.

	3A	3B	3C	3D	Total
Time (hr)		30			

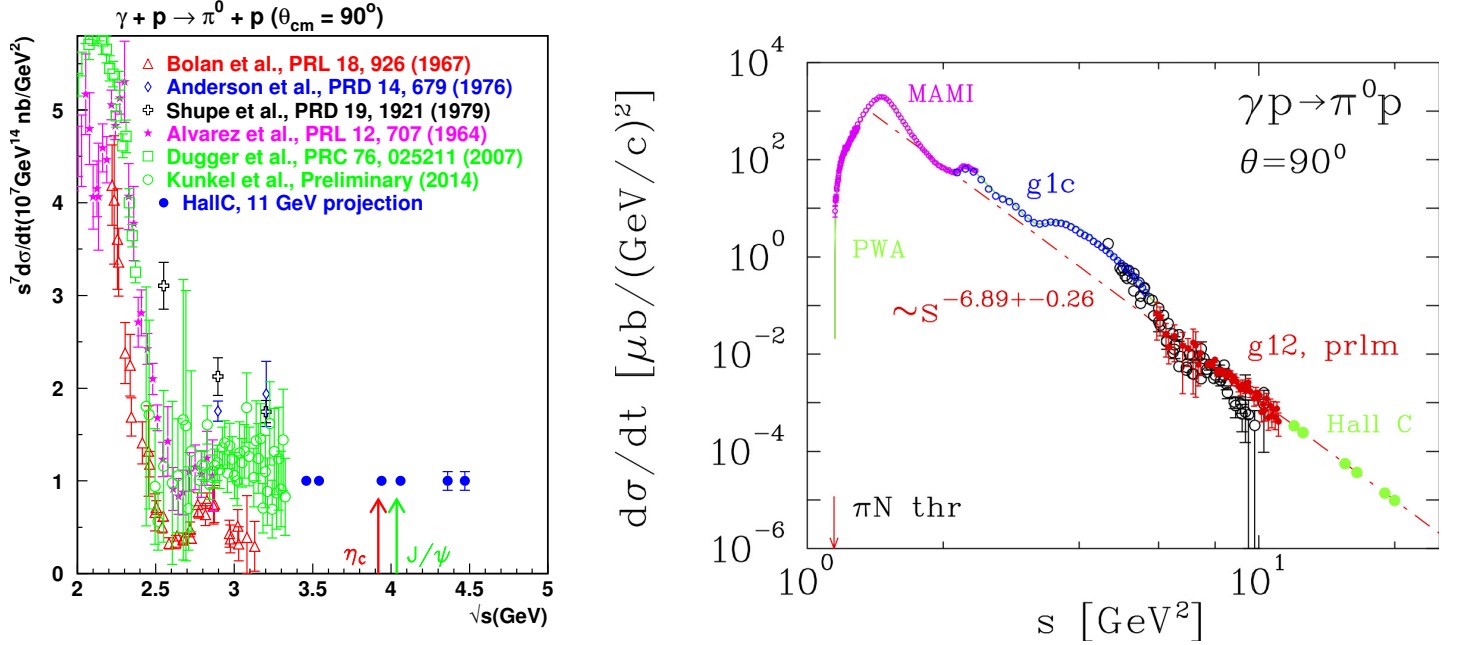


FIG. 19. Projected results at 90° C.M. angle.

The projected results for the ratios shown here are based on combining data from Hall-A and Hall-C. A 10% uncertainty assumed for both neutral and positive pions

SUMMARY

The $\gamma p \rightarrow \pi^0 p$ process is one of the simplest exclusive processes to investigate the dominance of the handbag mechanism, and to study the onset of scaling behavior for π^0 photoproduction. Utilizing fully the advantages of high luminosity and the energy upgraded CEBAF. The slower decrease of the differential cross-section for the process compared with many other photon induced two-body processes allows differential cross-section measurements all the way to the highest possible center-of-mass energy with a 11 GeV CEBAF beam. Specifically, a 11 GeV beam will allow:

- A precise measurement of the π^0 photoproduction cross section at the highest energies available, to help resolve some of the discrepancies between the previous measurements.
- When combined with π^+ measurements in Hall-A (to be collected as part of the calibration of the SBS spectrometer in for the G_E^n and G_M^n measurements), one can form the π^0/π^+ ratios that can be compared with GPD based models that have been successful in describing WCS [8]. These tests will help confirm the dominance of the handbag mechanism.
- Detailed investigation of the angular dependent scaling onset as observed in the deuteron photodisintegration process and to understand the origin of scaling behavior.

- Tests of generalized quark counting rule prediction and to investigate indirectly the effect of quark orbital angular momentum. And investigate the deviations from scaling behavior as shown in the proton-proton elastic scattering data and was suggested possibly by the E94-104 results [34].

•

-
- [1] X. Ji, Phys. Rev. Lett. **78**, 610 (1997); Phys. Rev. D **55**, 7114 (1997); A.V. Radyushkin, Phys. Lett. **B380**, 417 (1996); Phys. Rev. D **56**, 5524 (1997); M. Diehl, T. Feldmann, R. Jakob, P. Kroll, Eur. Phys. J. **C 8**, 409 (1999).
 - [2] A. V. Radyushkin, Phys. Rev. **D 58**, 114008 (1998) [hep-ph/9803316].
 - [3] M. Diehl, T. Feldman, R. Jacob, P. Kroll, Eur. Phys. J. **C 8**, 409 (1999) [hep-ph/9811253].
 - [4] H. W. Huang, P. Kroll, Eur. Phys. J **C 17**, 423 (2000) [hep-ph/0005318].
 - [5] N. Kivel and M. Vanderhaeghen, JHEP **04**, 029 (2013); arXiv:1212.0683; arXiv:1312.5456.
 - [6] H. W. Huang, P. Kroll, T. Morii, Eur. Phys. J. **C 23**, 301 (2002).
 - [7] M. Diehl and P. Kroll, Eur. Phys. J. **C 73**, 2397 (2013); arXiv:1302.4604.
 - [8] G. Eichmann and C. S. Fischer, Phys. Rev. D **87**, 036006 (2013); arXiv:1212.1761.
 - [9] H. W. Huang, R. Jacob, P. Kroll, K. Passek-Kumericki, Eur. Phys. J **C 33**, 91 (2004); P. Kroll private communication.
 - [10] R. Ent, T. Horn, H. Mkrtchyan *et al.*, Neutral-Pion Spectrometer Facility in Hall C, proposal to Jefferson Lab PAC 40.
 - [11] B. Wojtsekhowski, D. J. Hamilton, S.Širca *et al.*, Wide-angle Compton scattering at 8 and 10 GeV photon energies, proposal to Jefferson Lab PAC 41.
 - [12] R. Ent, T. Horn, H. Mkrtchyan *et al.*, Measurement of Semi-Inclusive π^0 Production as Validation of Factorization, proposal to Jefferson Lab PAC 40.
 - [13] C. White *et al.*, Phys. Rev. **D49**, 58 (1994).
 - [14] S.J. Brodsky and G.R. Farrar, Phys. Rev. Lett.**31**, 1153 (1973); Phys. Rev. D **11**, 1309 (1975); V. Matveev *et al.*, Nuovo Cimento Lett. **7**, 719 (1973);
 - [15] G.P. Lepage, and S.J. Brodsky, Phys. Rev. D **22**, 2157 (1980).
 - [16] T. Gousset, B. Pire and J. P. Ralston, *Phys. Rev. D* **53**, 1202 (1996).
 - [17] N. Isgur and C. Llewellyn-Smith, Phys. Rev. Lett. **52**, 1080 (1984).
 - [18] X. Ji, J.-P. Ma and F. Yuan, Phys. Rev. Lett. **90**, 241601 (2003).
 - [19] J. Polchinski and M.J. Strassler, Phys. Rev. Lett. **88**, 031601 (2002); R.C. Brower and C.I. Tan, Nucl. Phys. B **662**, 393 (2003); O. Andreev, Phys. Rev. D **67**, 046001 (2003).
 - [20] S. J. Brodsky and G. F. de Teramond, Phys. Lett. **B582**, 211 (2004); S. J. Brodsky *et al.*, Phys. Rev. D **69**, 076001 (2004).
 - [21] M. Fuchs *et al.*, Phys Lett B 368, 20 (1996); R. Beck *et al.*, Eur Phys J A 28S1, 173 (2006)
 - [22] Dugger *et al.*, PRC 76, 025211 (2007).
 - [23] Kunkel *et al.*, Preliminary (2014).
 - [24] J. Napolitano *et al.*, *Phys. Rev. Lett.* **61**, 2530 (1988); S.J. Freedman *et al.*, *Phys. Rev. C* **48**, 1864 (1993); J.E. Belz *et al.*, *Phys. Rev. Lett.* **74**, 646 (1995).
 - [25] C. Bochna *et al.*, *Phys. Rev. Lett.* **81**, 4576 (1998).
 - [26] E.C. Schulte, *et al.*, *Phys. Rev. Lett.* **87**, 102302 (2001);
 - [27] P. Rossi *et al.*, Phys. Rev. Lett. **94**, 012301 (2005); M. Mirazita *et al.*, Phys. Rev. C **70**, 014005 (2004).
 - [28] K. Wijesooriya, *et al.*, *JournalPhys. Rev. Lett.* **86**, 2975 (2001).
 - [29] K. Wijesooriya, *et al.*, *JournalPhys. Rev. C* **66**, 034614 (2002).
 - [30] W. Luo *et al.* *JournalPhys. Rev. Lett.* **108**, 222004 (2012)
 - [31] D. P. Owen *et al.*, Phys. Rev. **181**, 1794 (1969); K. A. Jenkins *et al.*, Phys. Rev. D **21**, 2445 (1980); C. Haglin *et al.*, Nucl. Phys. B **216**, 1 (1983).
 - [32] R.L. Anderson *et al.*, Phys. Rev. **D14**, 679 (1976).

- [33] “Photoproduction of Elementary Particles”, edited by H. Genzel, P. Joos and W. Pfeil pp16-268, (1973).
- [34] L. Y. Zhu *et al.*, Phys. Rev. Lett. **91**, 022003 (2003); L. Y. Zhu *et al.*, nucl-exp/0409018.
- [35] S. J. Brodsky, and G. F. de Teramond, Phys. Rev. Lett. **60**, 1924 (1988).
- [36] M. Dugger *et al.*, Phys. Rev. **C 76**, 025211 (2007).
- [37] W. Chen *et al.*, Phys. Rev. Lett. **103**, 012301 (2009).
- [38] M. Dugger *et al.*, Phys. Rev. **C79**, 065206 (2009).
- [39] R. A. Arndt, W. J. Briscoe, R. L. Workman, and I. I. Strakovsky, the GWU CNS Database, http://gwdac.phys.gwu.edu/analysis/pr_analysis.html
- [40] A. Sibirtsev, J. Haidenbauer, S. Krewald, T.-S. H. Lee, U.-G. Meissner, and A. W. Thomas, Eur. Phys. J. A **34**, 49 (2007); A. Sibirtsev (private communications).
- [41]
- [42]
- [43] P. V. Landshoff, Phys. Rev. D **10**, 1024 (1974).
- [44] A.W. Hendry, Phys. Rev. D **10**, 2300 (1974).
- [45] D.G. Crabb *et al.*, Phys. Rev. Lett. **41**, 1257 (1978).
- [46] G.R. Court *et al.*, Phys. Rev. Lett. **57**, 507 (1986), T.S. Bhatia *et al.*, Phys. Rev. Lett. **49**, 1135 (1982), E.A. Crosbie *et al.*, Phys. Rev. D **23**, 600 (1981).
- [47] S.J. Brodsky, C.E. Carlson, and H. Lipkin, Phys. Rev. D **20**, 2278 (1979).
- [48] A. Sen, Phys. Rev. D **28**, 860 (1983).
- [49] J. Botts and G. Sterman, Nucl. Phys. **B325**, 62 (1989).
- [50] A. H. Mueller, Phys. Rep. **73**, 237 (1981).
- [51] J.P. Ralston and B. Pire, Phys. Rev. Lett. **61**, 1823 (1988), J.P. Ralston and B. Pire, Phys. Rev. Lett. **65**, 2343 (1990).
- [52] C.E. Carlson, M. Chachkhunashvili, and F. Myhrer, Phys. Rev. D **46**, 2891 (1992).
- [53] Q. Zhao and F. E. Close, Phys. Rev. Lett. **91**, 022004 (2003).
- [54] A. V. Belitski, X. Ji and F. Yuan, Phys. Rev. Lett. **91**, 092003 (2003).
- [55] M. K. Jones *et al.*, Phys. Rev. Lett. **84**, 1398 (2000); O. Gayou *et al.*, Phys. Rev. Lett. **88**, 092301 (2002).
- [56] D. Dutta and H. Gao, Phys. Rev. **C 71**, 032201R (2005).
- [57] C. W. Akerlof, *et al.*, Phys. Rev. **159**, 1138 (1967); R. C. Kammerud, *et al.*, Phys. Rev. D **4**, 1309 (1971); K. A. Jenkins, *et al.*, Phys. Rev. Lett, **40**, 425 (1978).
- [58] L.L. Frankfurt, G.A. Miller, M.M. Sargsian, and M.I. Strikman, Phys. Rev. Lett. **84**, 3045 (2000), M.M. Sargsian, private communication.
- [59] P. Jain, B. Kundu, and J. Ralston, Phys. Rev. **65**, 094027 (2002).
- [60] G.R. Farrar, G. Sterman, and H. Zhang, Phys. Rev. Lett. **62**, 2229 (1989).
- [61] E. Anciant *et al.*, Phys. Rev. Lett. **85**, 4682 (2000).
- [62] B. Kundu, J. Samuelsson, P. Jain and J.P. Ralston, Phys. Rev. D **62**, 113009 (2000).
- [63] M. Kubantsev *et al.*. Performance of the Primex Electromagnetic Calorimeter, arxiv:physics/0609201, Sept 22, 2006; A. Gasparyan, Performance of PWO crystal detector for a High Resolution Hybrid Electromagnetic Calorimeter at Jefferson Lab, Proceed. X Int. Conf. on Calorimetry in Particle Physics, Perugia, Italy, 29 March - 2 April 2004, pp 109.
- [64] David J. Hamilton, A simulation of the 12 GeV Hall C RCS experiment, University of Glasgow, April 14, 2013 (unpublished).
- [65] Ren-yuan Zhu, Nucl. Instr. Meth. A **613** (1998) 297
- [66] C. Hyde-Wright, A. Nathan, and B. Wojtsekhowski, spokespersons, JLab experiment E99-114.
- [67] P.E. Bosted, Phys. Rev. C **51** (1995) 409.
- [68] Durham databse